Microfluidics and Nanofluidics (2021) 25:23
https://doi.org/10.1007/s10404-021-02425-y

RESEARCH PAPER

A 3D hydrodynamic flow-focusing device for cell sorting

Xiaofei Yuan[1,2] · Andrew Glidle[1] · Hitoshi Furusho[3] · Huabing Yin[1]

Received: 20 August 2020 / Accepted: 21 January 2021

Abstract
Optical-based microfluidic cell sorting has become increasingly attractive for applications in life and environmental sciences due to its ability of sophisticated cell handling in flow. The majority of these microfluidic cell sorting devices employ two-dimensional fluid flow control strategies, which lack the ability to manipulate the position of cells arbitrarily for precise optical detection, therefore resulting in reduced sorting accuracy and purity. Although three-dimensional (3D) hydrodynamic devices have better flow-focusing characteristics, most lack the flexibility to arbitrarily position the sample flow in each direction. Thus, there have been very few studies using 3D hydrodynamic flow focusing for sorting. Herein, we designed a 3D hydrodynamic focusing sorting platform based on independent sheath flow-focusing and pressure-actuated switching. This design offers many advantages in terms of reliable acquisition of weak Raman signals due to the ability to precisely control the speed and position of samples in 3D. With a proof-of-concept demonstration, we show this 3D hydrodynamic focusing-based sorting device has the potential to reach a high degree of accuracy for Raman activated sorting.

Keywords 3D flow-focusing · Multilayer structures · Cell sorting · Microfluidics · Raman

1 Introduction

With the capability of high throughput screening in cell sorting, traditional flow cytometer and fluorescence activated cell sorting (FACS) systems have become powerful tools for routine clinical and laboratory use (Bonner et al. 1972; Nolan et al. 1988). However, these techniques usually require target cells to be labelled and are thus not universally applicable. This is particularly true when label-free methods are desirable due to the time required to label the sample, the difficult to label efficiency and specificity, or adverse effects of the label on cell metabolism and viability. These concerns have led to increasing interest in techniques requiring no labeling, such as Raman spectroscopy (Kong et al. 2015), image analysis (Li et al. 2014; Yuan et al. 2017), or frequency dependent and cell-specific electrical impedance profiles (B. Y. Chang and Park 2010).

Other well-known drawbacks of conventional FACS instruments are associated with the complexity of the instrumentation, high capital and maintenance costs and the need for relatively large sample volumes. Microfabricated microfluidic flow cytometers and sorters are promising approaches to address these limitations (Shen et al. 2019; Yin and Marshall 2012). Here, advantage is taken of the typical dimensions of the microfabricated channels being compatible with those of biological cells and their fabrication being relatively simple. A further advantage of microfabricated devices is that they can be easily integrated with existing laboratory instrumentation. This leads to platforms that enable sophisticated cellular analyses and/or the isolation of target cells for post-processing (Skommer et al. 2013; Wolff et al. 2003).

Among the microfluidic-based cell sorting devices, sorting strategies include those that rely on inertial flow, viscoelastic flow, shear-induced diffusion (Di Carlo 2009; Zhou et al. 2019; Zhou et al. 2018a, b), and hydrodynamic focusing. For the latter strategy, two classes of device have been developed in attempts to precisely guide and position cells within a fluid channel network. One class is based on a substantially '2D' design, in which two sheath flows are placed either side of the sample stream containing the cells

✉ Professor Huabing Yin
huabing.yin@glasgow.ac.uk

[1] Division of Biomedical Engineering, School of Engineering, University of Glasgow, Glasgow G12 8QQ, UK

[2] School of Environmental Science and Engineering, Southern University of Science and Technology, Shenzhen 518055, China

[3] Nissan Chemical Corporation, Tokyo, Japan

Published online: 15 February 2021

to laterally focus it down to a size of 10′s μm (Skommer et al. 2013). This concept features in many applications where detection of the 'identification' signal used for the sorting process is easy due to its magnitude (e.g., strong fluorescence signals). However, 2D hydrodynamic focusing inherently lacks a high degree of control in the z-position of cells when they are flowing through the detection chamber of a device. This lack of z-positional control results in reduced sorting accuracy and purity in cases where the magnitude of the identification signal is close to the background signal levels and/or very sensitive to a cell's position, such as when the cell passes through the optical focus of a laser beam.

Furthermore, as with many microfluidic platforms, these 2D devices still suffer from limitations such as those associated with channel clogging (as occurs when slowly moving streams of adherent cells come into contact with the channel walls, for example), and a degradation in sorting performance when the cells are poorly constrained in the focussed flow due to their small size (Lu et al. 2014; Mao et al. 2007; Xu et al. 2011).

A second type of focusing structure uses 3D hydrodynamic control to constrain and position the cells. In general, this is done by creating either a cylindrical sheath flow profile (Lee et al. 2009; Nawaz et al. 2014) or using multiple sheath flows (C. C. Chang et al. 2007; Simonnet and Groisman 2005) around a central sample stream. In comparison to 2D focusing, the flow profiles of 3D focusing devices lead to a more tightly confined focus, thus helping prevent cells in the sample stream from coming close to the channel walls (Xu et al. 2011) and more tightly confining the focus.

Various architectures have been reported for hydrodynamic 3D focusing (Daniele et al. 2015) devices: a simple contraction–expansion array that only uses one sheath flow inlet (Lee et al. 2009; Nawaz et al. 2014) with the focusing occurring through the creation of secondary Dean flow; a groove-based relief pattern on one of the channel faces to transform a sheath flow from 2D to 3D and so realize confinement (Howell et al. 2008); and two sheath flows used in combination with chevron-grooves—here the performance is remarkably improved (Golden et al. 2009). A further type of 3D design uses a structure in which the streams from two side sheath channels merge with the sample channel at different heights, showing a limited constraining effect in the transverse directions (Chiu et al. 2013). To improve on this, a third sheath flow has been added into some designs either beneath (Xu et al. 2011) or beside (Mao et al. 2012a, b; Nawaz et al. 2014) the sample stream.

All the above designs have inherent strengths and weaknesses, most commonly they (i) generally lack the flexibility to arbitrarily position the focussed sample flow in x–y and z directions; (ii) require both the sample and sheath flow rates to be relatively high to achieve tight focusing, and (iii) lead to significant dilution of the sample with sheath flow solution downstream of the focus point. Factors (i) and (ii) are problematic in that they compromise the ability to collect signals from samples which would require long acquisition times due to their weakness (e.g., 100′s milliseconds for Raman signals) or where fine re-positioning of the microfluidic device is not possible after it has been inserted into a measurement apparatus. With factor (iii), excessive dilution of the sample makes recovery and post processing of collected target cells significantly more challenging when small numbers of cells are involved. Taken together, these difficulties may account for there being relatively few studies that use 3D hydrodynamic flow focusing for sorting. Those that have been reported are based on large fluorescence or colour absorption signals (Chen et al. 2013; Meineke et al. 2016), or, in the case of our recent work using a 3D printed flow-focusing device (Lyu et al. 2020), the first report of Raman-based sorting (using the 'Raman window' concept to maximise the signal).

As indicated above, Raman spectroscopy is a label-free and non-destructive technology. Raman spectra of single cells consist of rich Raman "fingerprints" formed from the sum of the spectroscopic features characteristic of each compounds within a single cell. This fingerprint can thus be used to characterise both cell phenotype and physiological functions (Wang et al. 2020). However, since spontaneous Raman signals are inherently weak, there are significant challenges when carrying out flow-based sorting and often spectra are instead acquired when the cells are momentarily held in a stationary position (Song et al. 2016). Potentially, the stop-and-measure strategy limits the throughput of a platform and consequently in the first study in this area, we demonstrated the principle of "trap-free" Raman activated cell sorting (McIlvenna et al. 2016) using a 2D hydrodynamic focusing method. However, during the course of that study we noted that the Raman signal from a bacterial cell could fall by over 50% with only ~ 5 μm change in the z-focus position of a high magnification objective (Fig. S1). This observation prompted the development of a 3D flow focusing strategy with precise control of the sample stream z-position to achieve high throughput and robust cell sorting.

In formulating a new 3D flow focusing strategy we sought to address the limitations (i)-(iii) outlined above. The aim was to develop a novel hydrodynamic 3D flow-focusing microfluidic method that could be used for either continuous fluorescence- or Raman-activated cell sorting. To do this, our scheme employed a straightforward design that included four independently controlled sheath flow inlet streams surrounding the sample stream, and four independently controlled sheath flow outlet streams that surrounded the sample outlet stream and were downstream of the flow focus point. These inlets and outlets provided both the degree of flow focusing and spatial positioning (in x−y and z) required. In addition, the downstream outlet channels served to convey

a substantial fraction of the sheath flow fluid away from the sample stream, before it enters a channel network that performs the cell sorting actuation. Although constructed with fluorescence or Raman detection in mind, these devices should result in systems with great flexibility in controlling flows in 3D for a variety of applications or platforms.

The basic design envisaged could be realised using either 3D printing or photolithographic techniques as best suited to particular scenarios. For example, when sorting relatively large cells from samples that are likely to clog the detection device, it might be appropriate to use a 3D printed structure that has a large volume detection chamber and which can be readily cleaned and re-used. However, when sorting relatively small cells (e.g., < 5 μm) from 'clean' (or debris free) solutions, a higher throughput fabrication technique such as photolithography, is more appropriate.

We have recently reported the method of implementation of the 3D focusing strategy using 3D printed devices (Lyu et al. 2020). Here, we report a route to create the 3D focusing devices that employs both positive and negative photoresists to build a suitable multiple-layer structure through a repetitive photolithography process (Yasukawa et al. 2005). Although not discussed here, this photolithographic route could also include additional fabrication steps to incorporate features used in other cell characterisation modalities, such as dielectrophoresis electrodes, on-chip PCR heaters, integrated optoelectronic elements, etc. Here, instead, to demonstrate the efficacy of the 3D hydrodynamic focusing-based cell sorting concept, we used a standard Raman microspectrometer to create a simple sorting platform based on identification of small features in a Raman spectrum rather than the Raman window approach used earlier.

2 Material and methods

2.1 Design of 3D flow-focusing device

A computational fluid dynamics (CFD) simulation using *COMSOL* software version 5.2a was carried out to verify the functionality of the conceptual 3D hydrodynamic focusing device described above. To avoid excessive computation, the simulation concentrated on the heart of the device comprising two pairs of inlet sheath flows used to confine the position of a central sample stream in both the lateral (i.e., y direction) and vertical (i.e., z direction) directions as it enters a detection chamber (i.e., the detection region) in the x direction (Fig. 1). As indicated above, the outlet sheath flow outlet channels enable excess sheath flow fluid to be removed before the sample stream enters a downstream microfluidic network, where target cells are sorted and then further processed or extracted for off-chip studies. The COMSOL modules used to perform the simulation were the inbuilt *Laminar Flow* and *Transport of Diluted Species* ones. Fluid flows in the simulations were controlled by applying uniform pressures to the faces of the inlet and outlet channels.

The channel dimensions used in the basic design simulation were based on the feature dimensions that could be fabricated reliably using conventional photolithography as well as cell sizes (here, 2 μm was considered). Typically these were 100 μm × 15 μm (width x height) for the top and bottom sheath flow channels and 100 μm × 100 μm for the side flow channels. The middle (sample flow) inlet and outlet channels had entrance/exit dimensions of 100 μm × 10 μm, narrowing down to 20 μm × 10 μm where these channels meet the detection chamber (see below).

Using the basic design of Fig. 1, a range of sheath and sample flow rates were explored to discover the conditions and channel sizes that could achieve a 3D flow focused sample stream that was ~ 10 μm wide, ~ 1–2 μm thick with the linear speed of cells in the middle of the detection chamber being ~ 1 mm/s. This is appropriate to a detection time of ~ 10 ms using a laser focus spot size of ~ 10 μm. Optimization of certain features in the design involved looking at how the streamline routes of the sample flow varied with different outline profiles of the SU-8 layer structure. Here, the overall aim was to create sample streamline profiles that focused rapidly to a small region at the centre of the chamber, with minimal expansion of the profile into the detection chamber. The tightest profiles realizable with the photolithographic procedures used, were obtained when the features in the SU-8 pattern that defined the sample channel walls at the detection chamber inlet was tapered from 100 μm wide down to 20 μm.

The simulation of Fig. 1 shows the flow profiles resulting when the pressures applied to the side sheath flow inlet and outlet channel entrances/exits are 85 Pa and 75 Pa, respectively, ~ 600 Pa is applied to the top and bottom sheath flow inlets with the corresponding outlets being held at close to zero pressure. When ~ 100 Pa is applied to the sample inlet the sample flow rate into the chip is ~ 0.1 nl/s and the linear flow rate at the centre of the focused flow is ~ 1 mm/s (The flow rates in the side and top/bottom sheath flow channels are 0.1 μl/s and 0.015 μl/s, respectively.)

2.2 Fabrication of the 3D focusing device

The 3D microfluidic device was constructed on a glass slide using layer-by-layer photolithographic patterning of the positive photoresist AZ4562 (MicroChemicals GmbH, Germany) and the negative photoresist SU8-3025 (MicroChemicals GmbH), alternately (Fig. 2). This assembly is then coated with a photo-patternable silicone elastomer layer (see below). In this scheme, the patterned AZ resist layers are sacrificial ones which, after being eluted, define the sheath and sample flow channels of the final device

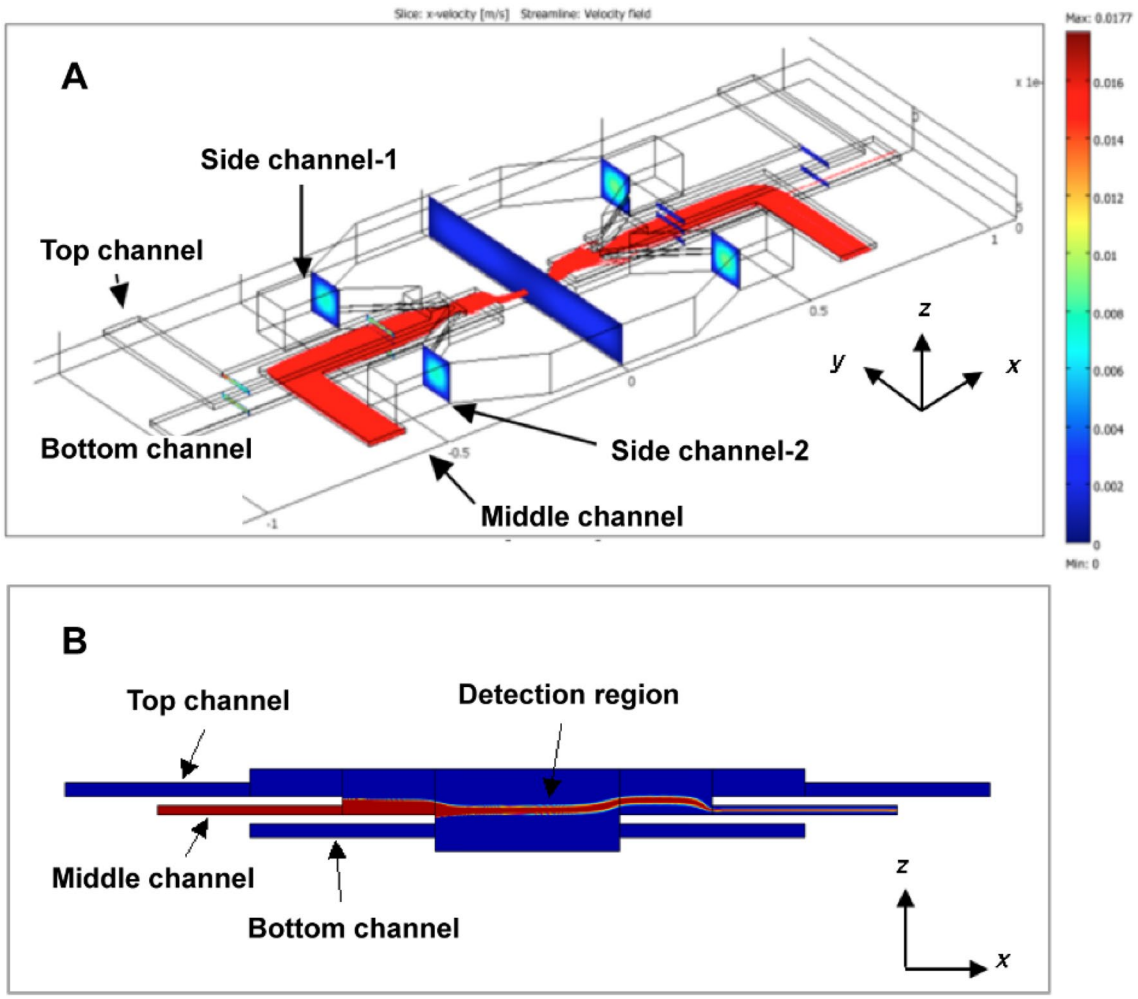

Fig. 1 **a** Schematic diagram of 3D hydrodynamic focusing device. The blue coloured planes indicate the flow velocity in the side channels and detection chamber, with the sample stream being shown through superposition of a high density of streamlines originating from the middle, sample, channel inlet (indicated red). **b** Cross-section along the mid-line of the device showing the simulated flow distribution, again with the sample flow (red) being shown through superposition of a large number of streamlines. The white space in between the blue and red coloured layers of the sheath flow and sample channels correspond to the solid parts of the 3D device (i.e., the SU-8 resist layers). See text for parameters used in simulation

(Yasukawa et al. 2005). The AZ layer thickness for the top and bottom (sheath flow) channels was ~ 16 µm and for the middle (sample flow) channel ~ 26 µm. The SU8 layers that serve as spacers between channels and define the channel structure in the final device were all ~ 22 µm thick (Fig. 2a). Other relevant dimensions of the main channel, side channels and detection region can be found in Supplementary Fig. S2.

To seal the top of the device with a simple PDMS covering, a layer of WL-5150 photo-patternable silicone (Dow Corning Corp., MI) was used as an effective PDMS compatible 'glue' (PDMS does not adhere well to SU-8). The WL-5150 was spin-coated on to the photo-patterned but undeveloped topmost SU8 layer (SU8-3, Fig. 2b). It was then photo-patterned itself before being developed in EC solvent together with the SU8-3 layer (MicroChemicals GmbH). Subsequently, the whole device was soaked in acetone for ~ 30 min to remove the sacrificial AZ layers, so forming a clear microfluidic channel network.

Finally, the soft PDMS covering that provided the 'lid' of the device was made from a 20:1 mixture of PDMS prepolymer and curing agent (Sylgard 184; Dow-Corning) to facilitate bond to the underlying WL-5150 silicone layer and cured at 80 °C for 20 min. Before bonding to the SU-8 channel structure, a biopsy punch was used to create 0.7 mm diameter inlet and outlet holes in the PDMS lid. Both the PDMS lid and the WL-5150 coated SU-8 device were oxygen plasma treated (100 W, 30 s) prior to bonding together to make the enclosed microfluidic 3D focusing and sorting platform (Fig. 2b).

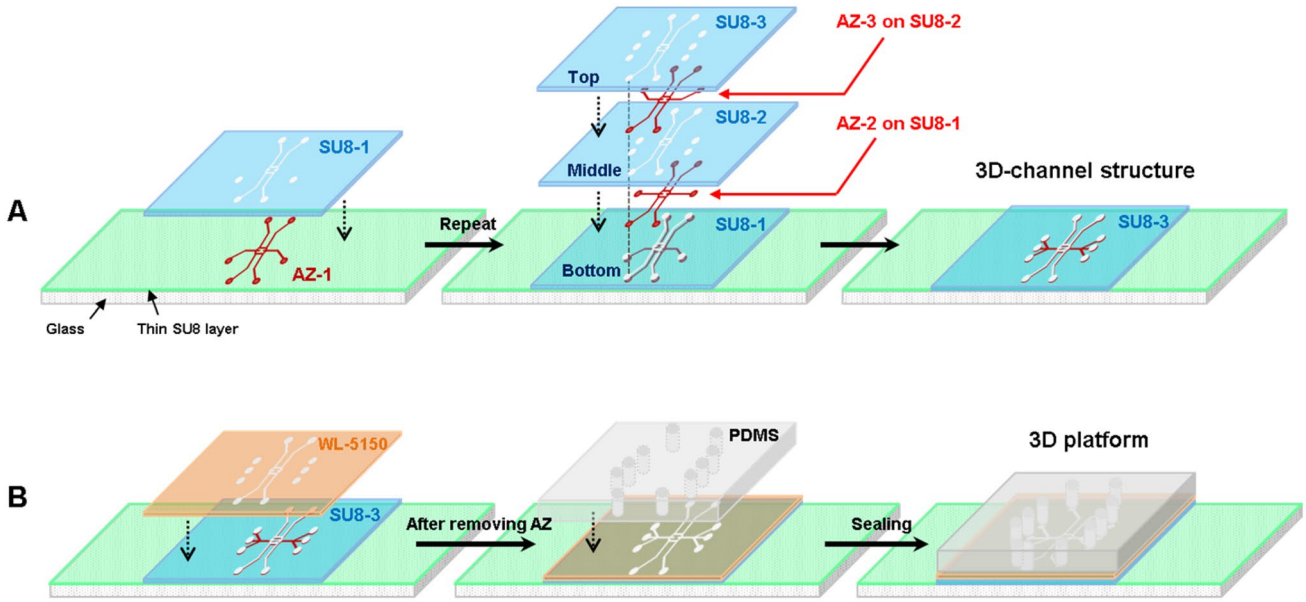

Fig. 2 **a** Scheme for fabrication of 3D microfluidic platform by patterning both AZ4562 and SU8-3025 photoresists, and (**b**) scheme for bonding the 3D platform to a PDMS slab after removal of the AZ photoresist through elution in acetone

2.3 Evaluation of 3D focusing performance

An inverted laser scanning confocal microscope (LSM 510, Carl Zeiss Inc., Germany) was used to evaluate flow focusing effect of the 3D focusing device. Water and rhodamine B (1 mM solution) served as the sheath and sample flows, respectively. For the purposes of evaluating 3D focusing performance, these were delivered into the top and bottom channels and the middle one using syringe pumps (NE-1000, New Era Pump Systems Inc.) with the side sheath flow channels being fed using a hydrostatic-based pressure system. The reason for using hydrostatic control for the side channels was so that the relatively small pressure difference required to generate the desired flow rates could be both maintained in a stable fashion and small changes could be made by simply adjusting the difference in height of the liquid levels in the reservoirs connected to the inlet and outlet side sheath flow channels. However, it should also be noted that in normal operation either high quality syringe pumps, good quality microfluidic pressure control units (e.g., Fluigent systems) could be used in place of hydrostatic control if desired.

For confocal measurements, the laser beam ($\lambda = 543$ nm) was initially focused on the rhodamine B stream in the detection chamber and then scanned to record three-dimensional images through a 20×/0.45 NA objective lens, with z-slices acquired 1 µm intervals.

2.4 Raman-activated sorting

Raman-activated sorting was performed on a Horiba Jobin–Yvon HR800 Raman microspectrometer fitted with a Horiba Jobin–Yvon Synapse CCD camera and a Quantum Laser Torus 532 nm laser. Spectra were acquired with either a 50x/0.55 NA or 63x/0.7 NA objective, a pinhole of 300 µm and a 600 groove/mm grating. The grating position was adjusted so that the Raman spectra collected were centred around 1300 cm^{-1}. To control sorting and spectra acquisition, a custom *Labview* programme was developed. This enabled synchronisation of Raman detection, on-the-fly spectral classification and pressure control (MFCS, FLUIGENT GmbH, Germany) as required for automated Raman-activated sorting (previously described in (McIlvenna et al. 2016)). Here, pressure-driven actuation was used to perform the sorting actuation since it is simple and widely applicable to many applications.

To provide a model system to demonstrate the sorting capabilities of the microfluidic device, solutions 0.001% 6.5 µm diameter Flash Red or Dragon Green fluorescent polystyrene spheres (Bangs Laboratories, Inc., IN) in deionized water were sorted based on their Raman spectrum. The flow rates used for this demonstration varied from 1 to 0.2 mm/s, corresponding to maximum transit times through the laser spot of ~ 0.01 s and ~ 0.1 s, respectively. Although these beads are fluorescent, they also have a Raman signature

and could thus be observed at the switching junction and recorded in real time using a fluorescence imaging microscope positioned above the device.

3 Results and discussion

3.1 Simulations with COMSOL

A series of simulations were performed by varying the fluid pressure at the inlet or outlet of the individual channels and it was noted that Pouseille flow profiles developed rapidly before the corresponding fluid stream entered the detection chamber, as expected. These simulations showed that independent control of the flow rates of each of the top, bottom and side sheath flow streams could be used to provide focusing and positioning control in both the vertical and horizontal directions. In comparison to angled sheath flow structures used in other devices to achieve vertical focusing (Chiu et al. 2013; Daniele et al. 2015), which affects the horizontal focus position and shape in an independent and arbitrary fashion, this design provides unique flexibility in being able to simply adjust the z-position and shape of the focus as desired.

As an example of the simulations performed, Fig. 3 shows the sensitivity of this positioning to pressure differences in the various sheath flow channels. These show that position of the focus could be moved by distances of up to 10′s microns by adjusting the sheath flows using pressures that are all comfortably within those that can be stably generated by simple hydrostatic pressure, good quality microfluidic pressure systems, or good quality syringe pumps.

Additional insights gained from the modelling included an examination of the sheath flow streamlines (not shown in Fig. 1) that showed that after passing through the detection chamber, each of the sheath flow streams is directed to corresponding outlets with the focused sample flow being directed into the central outlet for cell sorting (the sorting network is not shown in Fig. 1, see Fig. 4 later) and that scaling the inlet and outlet pressures is all that is required to get flow focused cross sections of the order of 10 µm or less with low linear sample flow rates of ~ 0.01 mm/s in the detection chamber.

The feature of stripping away of a substantial fraction of the sheath flow focusing solution via the corresponding outlet channels achieves the goal of reducing excessive sample dilution that would otherwise occur between the detection point and the downstream cell switching module. For example, with the configuration above, simulations show that the concentration of entities in the sample inlet are diluted by a factor of ~ 12 when entering the sample outlet channel; if instead a device is modelled in which a 25 µm diameter sample stream is surrounded by 100 µm thick sheath flow channels on all four sides, and the flow rates are adjusted to give a 10 µm focused flow, the sample is diluted by a factor of over 400 downstream of the flow focus point.

When comparing the flow rates used in other hydrodynamic focusing systems with the system here, whilst those indicated in the simulations above might appear low (0.1 nl/s for the sample flow in the above simulation), this is commensurate with that which would be expected for any system in which the

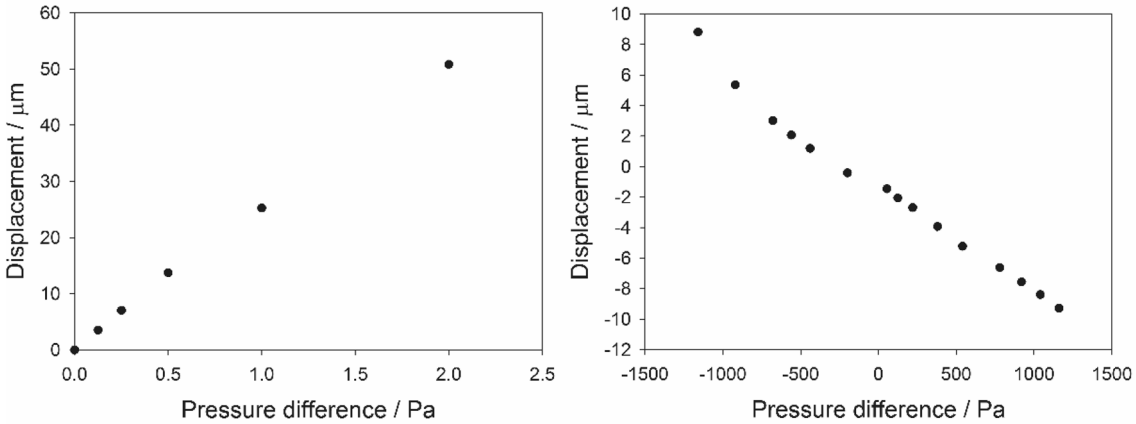

Fig. 3 Left: Displacement of flow focus in the lateral (y-axis) direction as a consequence of imposing different pressures on the side sheath flow channel inlets. Zero lateral displacement corresponds to a side sheath flow inlet pressure of 85 Pa and side flow outlet pressure of 75 Pa; a pressure difference of 2 Pa corresponds to adjusting one side sheath flow inlet pressure to 86 Pa and the other to 84 Pa, with the corresponding outlet sheath flow pressures being adjusted to ~ 74 Pa and ~ 76 Pa to ensure the sample continues to flow into the collection channel. Right: displacement of flow focus in the vertical (z-axis) direction as a consequence of imposing different pressures on the top and bottom sheath flow channel inlets. Zero displacement corresponds to a position 25 µm above the base of the detection chamber and a positive pressure difference corresponds to the top sheath flow pressure being greater than the bottom sheath flow pressure

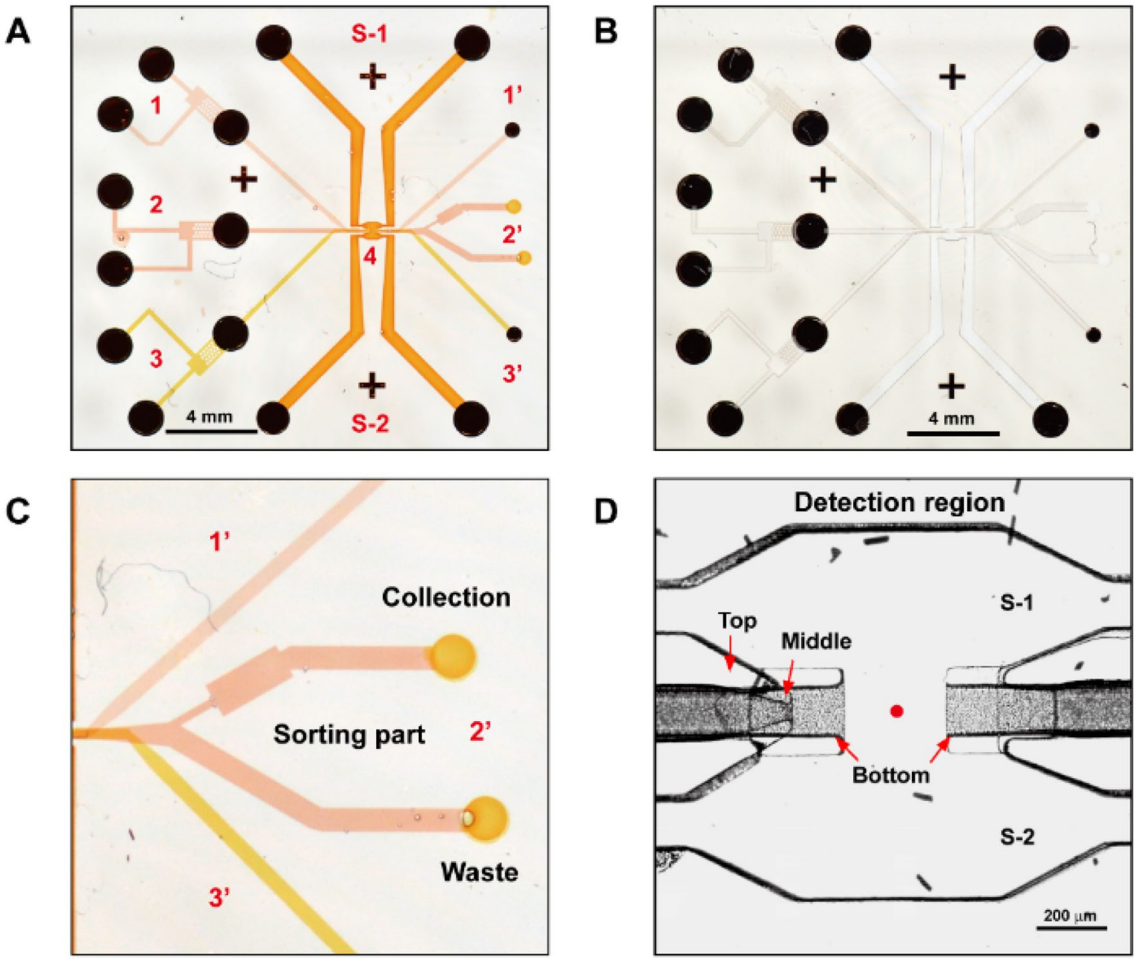

Fig. 4 Photographs of the whole 3D-focusing microfluidic structure before (**a**) and after (**b**) removing the AZ photoresist. The different yellow-orange-red colours of the AZ resist defined channels reflect the degree to which they have been exposed to UV light in successive steps of the scheme in Fig. 2a. The labels 1, 2 and 3 correspond to inlets of the top (sheath), middle (sample) and bottom (sheath) channels, and 1′, 2′ and 3′ their outlets. S-1 and S-2 represent the two side (sheath flow) channels and label 4 designates the location of the detection chamber. **c** Magnified structure of collection and waste channels used for sorting. **d** Micrograph of detection chamber after elution of the AZ resist. Red arrows show the ends of the top (sheath), middle (sample) and bottom (sheath) channels in the vicinity of the detection zone. The red dot indicates the optimal detection position created by the sheath flow focusing

linear flow of the sample at the detection point was restricted to 1 mm/s (i.e., a 10 µm cross section fluid stream travelling at 1 mm/s corresponds to a volumetric flow rate of 0.078 nl/s). However, this flow rate is considerably lower than those reported in 3D flow focusing systems such as the 0.5 µl/s in the work of Mao et al. (Xiaole Mao et al. 2012a, b) or 1.5 µl/s in the work of Lee, M.G et al. (Lee et al. 2009). Thus for both of those reported flow rates, either the focused spot size or speed of the solution going through the focus point would need to be several orders of magnitude larger than those used here, neither of which are compatible with the Raman-based applications envisaged here. Similarly, in reported Dean flow-based cell sorting devices such as that of Zhou et al. (Yinning Zhou et al. 2018a, b), the sample flow rates are ~ 1–3 µl/s, which would again lead to much larger cell velocities.

3.2 Particular design features in the 3D device

The overview of the 3D focusing device before and after removing the sacrificial AZ layers is shown in Fig. 4a, b. Near to each of the inlets (1–3), there is a microfabricated pillar-based filter to prevent large sized debris from entering the microchannel network of the device. Fig. 4c shows the pressure-controlled sorting feature incorporated into the sample channel outlet arm. In the magnified detection region (Fig. 4d), the bottom, middle and top channels are all 100 µm wide and are well aligned in the x–y plane, with accurate vertical stacking in the z-direction. The use of such terracing in the design avoids misalignment during microfabrication, which could lead to leakage, cross-flow between the embedded channels or sealed/blocked ends to either the

sample or top and bottom sheath flow channels. This terracing strategy made the fabrication method very robust and reliable.

Two other notable aspects of the design are (i) the middle inlet channel has a progressively narrowing end designed to aid the focusing of the sample flow in the detection chamber (referred to in the simulation details above) and (ii) the side sheath flow channels were constructed so that their heights were equal to the combined thickness of the SU-8 layers (i.e., ~ 150 µm). This latter feature is because slightly greater focussing in the x–y plane compared to the z-direction is needed for applications in Raman microspectroscopy and the larger side channels facilitate the flow of a larger volume through without significantly increasing the internal stress between the patterned SU-8 layers.

3.3 Experimental control of the size, shape and position of the focussed sample flow

To demonstrate flow focusing indicated by the simulations above, experiments were performed to control the focus in both the lateral and horizontal directions independently (Fig. 5). Firstly, for control in the lateral direction, the sheath flow in the top and bottom channels was stopped. The flow

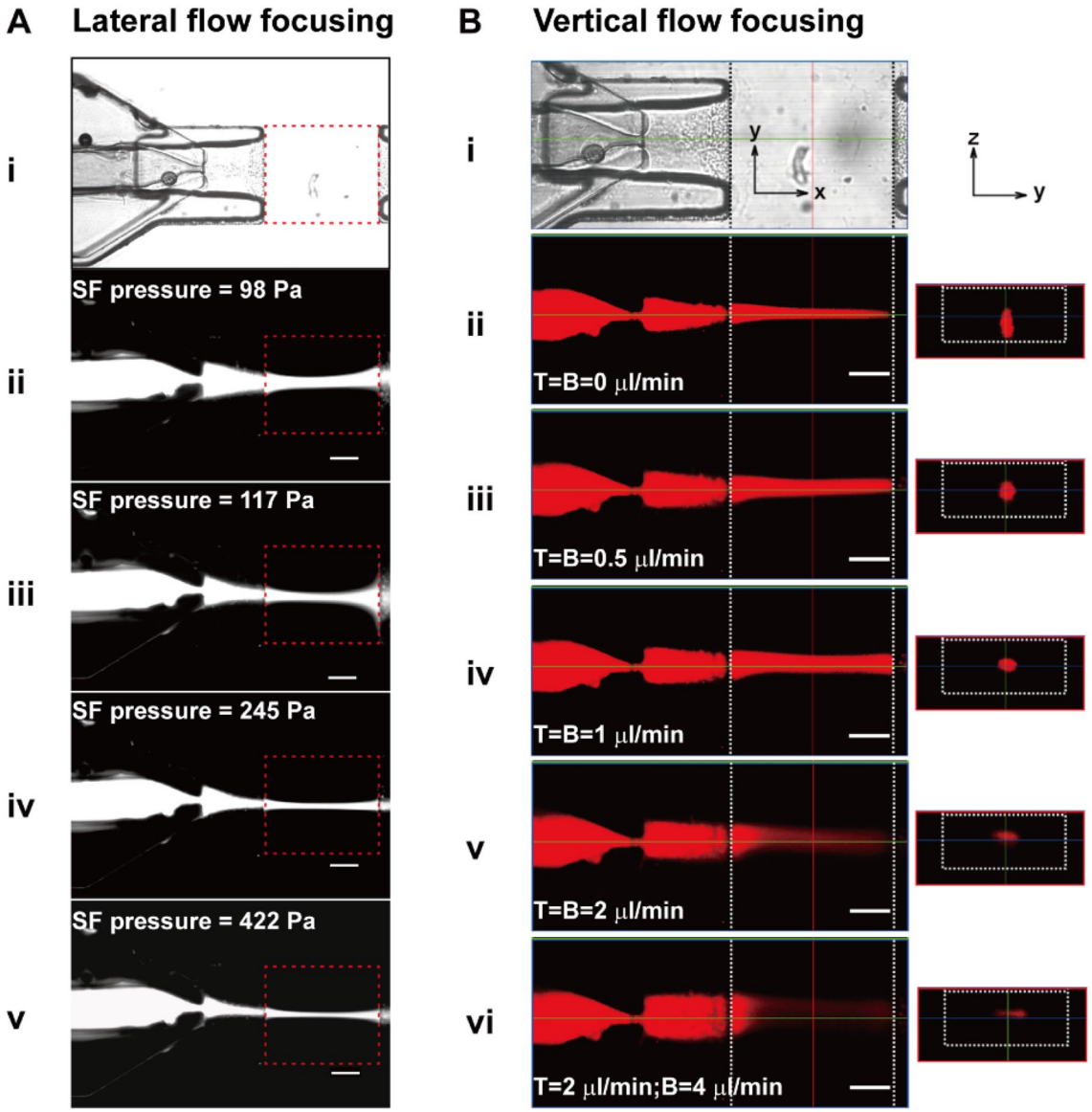

Fig. 5 **a** Lateral flow focusing control: (i) Bright field image of the detection region (the dotted red box). (ii) to (v) Fluorescence images viewed from above of a rhodamine B sample flow confined solely by side sheath flows (SF), at gradually increasing hydrostatic pressures, shown inset in each image (see text for details). Scale bar is 200 µm. **b** Vertical flow focusing control: (i) Bright field image of the detection region. (ii) to (vi) Confocal images of the rhodamine B sample flow in the x–y and y–z planes. The y–z profile at the cross-section indicated by the dotted red line in B(i) is shown adjacent to each image. T denotes top sheath flow rate; B denotes bottom sheath flow rate. Scale bar is 100 µm

rate of the sample stream containing the rhodamine B solution was fixed at 0.05 µl/min using a syringe pump and the side sheath flow pressures were controlled hydrostatically. As expected, no flow-focusing occurred until the side sheath flow pressure increased above a certain level, Fig. 5a. On increasing the side sheath flow rate the sample stream gradually focusses in the horizontal direction generating the narrow sample flow pattern observed in the sequence of images in Fig. 5a. Here, the width of the focused sample flow stream reduces from 72 µm to 51, 36 and 27 µm, respectively as the hydrostatic pressure difference between the inlet and outlet of the side sheath flow channels rises from 98 Pa to 117, 245, and 422 Pa (Fig. 5a ii–v). (Note, these pressure differences are larger than those shown in the simulations of Figs. 1 and 3 due to the pressure drop along the tubing leading from the fluid reservoirs to the device inlets.)

Secondly, vertical focusing performance was evaluated via adjusting the top and bottom sheath flow rates, using a sample flow rate of 0.05 µl/min and side sheath flow pressure difference of 422 Pa. For these conditions the fluorescence profiles along the flow axis (x–y) and perpendicular to the flow axis (y–z) are shown in Fig. 5b. Fig. 5b-ii shows that when there was no flow in the top and bottom sheath flows, the flow profile generated by the side sheath flow streams nevertheless generated some degree of focusing of the rhodamine B stream in the z direction, (the z-y view to the right of the main image, shows that the fluorescent stream is slightly constrained in the vertical direction). However, as the top and bottom sheath flows are increased to 0.5 µl/min or 1 µl/min, the sample stream becomes well confined in the vertical direction and, as a result, the y–z profile of the rhodamine B stream appears properly focused in the centre of the detection chamber (Fig. 5b iii–iv). Further increases in the top and/or bottom sheath flow rates thereafter squeeze the sample stream into a thinner strip, at the expense of an increase in its lateral width (Fig. 5b v–vi). Thus, the vertical and lateral focusing forces can be easily balanced to achieve either a close to circular cross section for the sample flow or other shaped profile, as desired.

Thirdly, an illustration of how the focused sample stream can be steered away from the midline of the device using different pressures (or flow rates) applied to the side sheath flow streams (corresponding to the simulations of Fig. 3) is provided in Fig. S3).

Finally, since the sample stream flow rate is significantly slower than that of the sheath flows, the cross section of the focus can be reduced or increased in size by simple adjustment of the sample flow rate without the need for significant adjustment of the sheath flow rates. It was also found that by appropriate adjustment of the sheath and sample flow rates or pressures, the linear speed of the cells in the detection chamber can be adjusted from values as low as 0.01′s mm/s up to ~ 10′s mm/s whilst maintaining a well-focussed flow profile, offering utility in both fast detection of strong signals (e.g., fluorescence) or slow detection for weak signals that require a long period of signal acquisition (e.g., Raman).

3.4 Integration 3D hydrodynamic detection and downstream sorting

Besides focusing, this multi-layered device possesses the ability to control the trajectory of the focused stream by tuning the sheath flow rates individually to steer the sample stream into any downstream outlet channel as desired, e.g., following a trigger signal from cell detection software indicating a target cell has passed through the detection zone. This kind of flexibility in controlling the flow stream is illustrated in Fig. 6, where the sample stream can be directed to

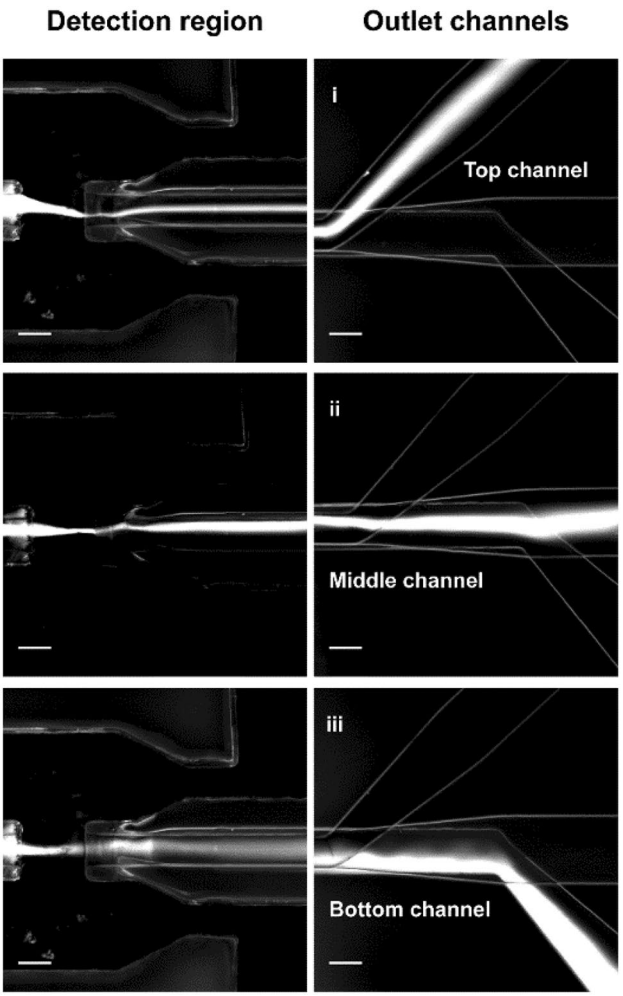

Fig. 6 Fluorescence images of a flow focused rhodamine B stream in the detection region (left), and after being directed to flow into different outlet channels (right) via independent control of the top (T) and bottom (B) sheath flow rates. Top and bottom sheath flow rates are (i) $T=0$ µl/min, $B=5$ µl/min; (ii) $T=1.2$ µl/min, $B=0.7$ µl/min; (iii) $T=8.5$ µl/min, $B=0$ µl/min. Flow rate of rhodamine B is 0.1 µl/min and the scale bar is 200 µm

either the middle collection channel, or one of the top and bottom sheath flow outlet channels. An advantage of this feature can be seen in the practicalities encountered in long duration experiments where, for example, it is to temporarily interrupt the sorting process to replenish sample or sheath flow solutions (or make other instrumental adjustments). In these cases, the pressures of the sheath flow streams can be altered to divert the sample stream into one of the sheath flow outlet channels, and so avoid potentially contaminating portions of a sample that have already been sorted.

However, during the routine course of sorting cells (or other entities), it is important switch cells into either collection or waste channels in such a manner as to not disturb the position of the focus flow in the detection chamber. The ease of such sorting actuation at a more downstream location (see Fig. 4c) is illustrated in Fig. 7 and Supplementary videos 1 and 3). Rhodamine B is used here as an easy means to visualise the trajectory of a target cell being diverted into one or other of two downstream outlets, as dictated by either the waste or collection outlet channel pressures, triggered by the sorting software. Such changes in the outlet pressures of the waste and target cells channels are shown in Fig. 7b, c to direct the sample flow to one or other destination. The lack of perturbation of the focused flow in the detection chamber during these switching events can be visualised by observing the rhodamine B flow profile there and is graphically illustrated in Supplementary Video 1. (In this video, the automated pressure switching is simulated using a repetitive, oscillatory movement of the head height of reservoirs connected to the two sorting channel channels.). Thus, the 3D hydrodynamic focusing function integrates well with a downstream sorting mechanism, in a single device without either disturbing the other's function.

3.5 Raman-activated sorting

To demonstrate the utility of this device in the field of Raman sorting, a proof-of-concept experiment was carried out using microspheres. As discussed above, precise and consistent delivery of cells to a tightly focussed laser spot at detection point is crucial to obtain Raman signals of sufficient magnitude to be detected. For easy in situ monitoring of the positional stability of a focussed sample stream in the absence of a fluorescent dye (which would interfere with any Raman measurements), green fluorescent beads of 6.5 µm in diameter were used. As shown in Fig. 8 and Supplementary Video 2, individual beads in the focused stream pass through the interrogation point of the focused laser beam with good consistency.

Raman-activated sorting was then conducted with the same beads after mixing with a solution of non-fluorescent beads of a similar size. For this mixture, a resonance Raman signal is generated when the fluorophore in the 'green' beads is stimulated by the 532 nm laser, with a series of Raman bands being observed in the region from 1000 to 1600 cm^{-1}. Figure 9 shows a Raman-activated cell sorting control

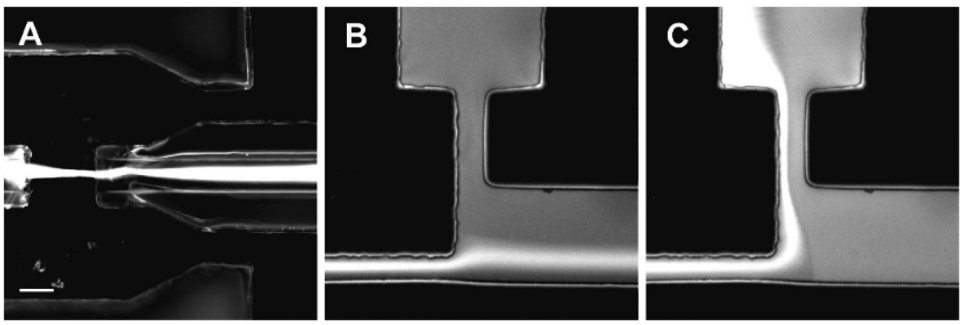

Fig. 7 **a** Fluorescence images of the stable sample flow of rhodamine B at the detection region during downstream switching to different outlets by changing the outlet pressure (*B* and *C*). The scale bar is 200 µm

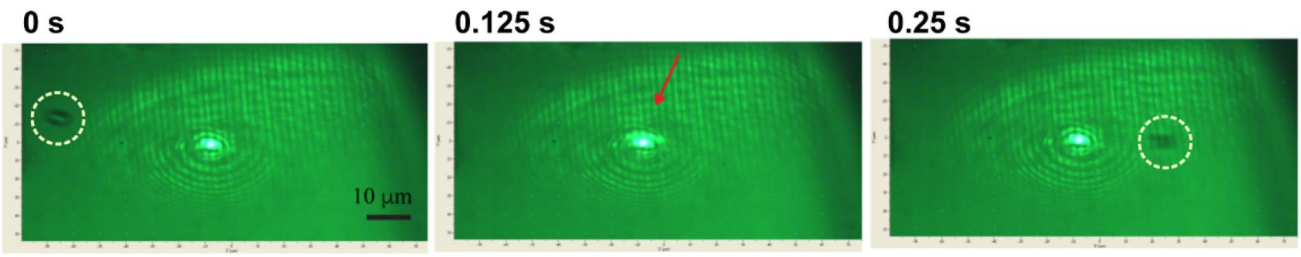

Fig. 8 Representative images of a bead (in the circle shown in the 0 s and 0.25 s frames) passing through the detection point where the laser spot was located. When the bead was close to (or in) the centre of laser spot (indicated by red arrow) at 0.125 s it was not visible due to the brightness of the laser. Flow rate of the bead is ~ 300 µm/s and the images show the x–y plane of the device, with the slight angle in the bead's trajectory being due to the orientation of the overhead camera used to collect the video sequence. (Supplementary Video 2)

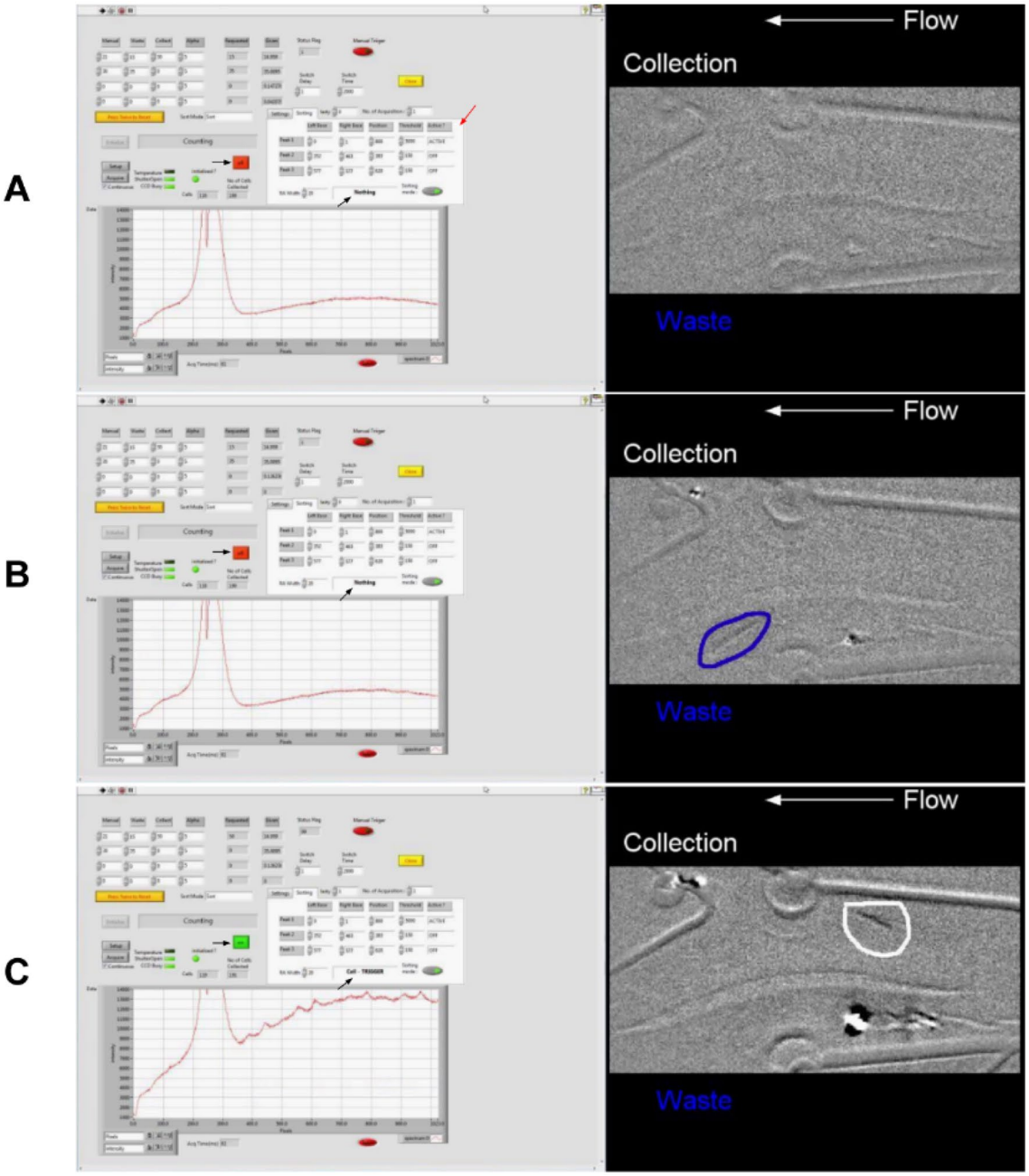

Fig. 9 Representative images to show the continuous Raman-activated sorting process. In each image, the Raman spectrum in the left panel is associated with the video frame in the right panel through synchronization of Raman acquisition and optical recordings. The red arrow in (**a**) shows where the Raman selection criteria are set in the software, and the black arrows in (**a**)-(**c**) show the status of sorting process in real time, i.e., the red button show in (**a**) and (**b**) means "sorting off" and the green button in (**c**) means "sorting on" (due to the identification of a target bead, shown in the adjacent video frame). In the video frames of (**b**) and (**c**) the blue and white circles show the beads moving to either the waste (non-target) or collection (target) channels, respectively, as also indicated by the sorting status shown in the corresponding panel on the left. Videos were recorded using an overhead microscope equipped with an Andor 885 CCD and bright field reflected light imaging (Supplementary Video 3)

program, through which the sample stream containing a bead is directed to the waste channel if the bead's Raman spectrum does not meet the selection criteria (as in Fig. 9a, b). In contrast, if designated features in the Raman spectrum are detected when a bead passes through the laser spot (Fig. 9c), the pressure actuated sorting process is triggered leading to the bead being directed to the collection channel.

To evaluate the reliability of the sorting process both Raman acquisition at the detection point and the channel into which the beads flow at the sorting junction were monitored

synchronously. From the short video of the software window in Video 3, eight beads met the criteria for collection (this corresponds to the "Number of cells collected" in the *Labview* front panel increasing from 188 to 196, and eight "cell-TRIGGER" commands being displayed). In the corresponding video sequence on the right side of the frames in Video 3, eight beads can be observed being directed to the collection channel immediately after each "cell-TRIGGER" command, with fifteen non-target beads going to the waste channel because their Raman spectra did not meet the sorting criteria (i.e., Raman peaks at a certain position and of a certain magnitude). This clearly indicates that the sorting platform has high accuracy for the collection of targeted entities in sample that meet the selection criteria. Note, that as with other cell sorting systems, the sorting accuracy will be dependent on many criteria. These include the magnitude of the Raman spectrum, the speed or time taken for target cells to travel from, the response time of the pressure switch used to divert the sample stream, and the likelihood of a target and non-target cell being sufficiently close together within the sample stream that they are switched together.

4 Conclusions

We successfully designed and fabricated a 3D flow-focusing microfluidic sorting device, which allows independent adjustment of sample and sheath flows in both flow rate and flow direction. It enables the precise delivery of a sample flow that is spatially and temporally stable, as is essential for acquisition of weak signals (e.g., Raman signals). The design also avoids significant dilution of the sample stream after it is collected downstream of the detection zone, and prevents any downstream pressure fluctuations as a consequence of sorting processes from disturbing the sample flow profile in the detection chamber. In addition, a high sorting accuracy was achieved in a proof-of-concept demonstration. All these unique advantages demonstrate the potential of this 3D flow-focusing design for accurate and robust cell sorting utility.

Supplementary Information The online version contains supplementary material available at https://doi.org/10.1007/s10404-021-02425-y.

Acknowledgements We thank Nissan Chemical Industries, Ltd. and NERC grants NE/P003826/1 and NE/S008721/1 for financial support and the technical support in the James Watt Nanofabrication Centre at the University of Glasgow.

References

Bonner WA, Hulett HR, Sweet RG, Herzenberg LA (1972) Fluorescence activated cell sorting. Rev Sci Instrum 43(3):404–409. https://doi.org/10.1063/1.1685647

Chang CC, Huang ZX, Yang RJ (2007) Three-dimensional hydrodynamic focusing in two-layer polydimethylsiloxane (PDMS) microchannels. J Micromech Microeng 17(8):1479–1486. https://doi.org/10.1088/0960-1317/17/8/009

Chen Y, Wu TH, Kung YC, Teitell MA, Chiou PY (2013) 3D pulsed laser-triggered high-speed microfluidic fluorescence-activated cell sorter. Analyst 138(24):7308–7315. https://doi.org/10.1039/c3an01266b

Chiu YJ, Cho SH, Mei Z, Lien V, Wu TF, Lo YH (2013) Universally applicable three-dimensional hydrodynamic microfluidic flow focusing. Lab Chip 13(9):1803–1809. https://doi.org/10.1039/c3lc41202d

Daniele MA, Boyd DA, Mott DR, Ligler FS (2015) 3D hydrodynamic focusing microfluidics for emerging sensing technologies. Biosens Bioelectron 67:25–34. https://doi.org/10.1016/j.bios.2014.07.002

Di Carlo D (2009) Inertial microfluidics. Lab Chip 9(21):3038–3046. https://doi.org/10.1039/b912547g

Golden JP, Kim JS, Erickson JS, Hilliard LR, Howell PB, Anderson GP, Nasir M, Ligler FS (2009) Multi-wavelength microflow cytometer using groove-generated sheath flow. Lab Chip 9(13):1942–1950. https://doi.org/10.1039/b822442k

Howell PB, Golden JP, Hilliard LR, Erickson JS, Mott DR, Ligler FS (2008) Two simple and rugged designs for creating microfluidic sheath flow. Lab Chip 8(7):1097–1103. https://doi.org/10.1039/b719381e

Kong K, Kendall C, Stone N, Notingher I (2015) Raman spectroscopy for medical diagnostics—from in-vitro biofluid assays to in-vivo cancer detection. Adv Drug Deliv Rev 89:121–134. https://doi.org/10.1016/j.addr.2015.03.009

Lee MG, Choi S, Park JK (2009) Three-dimensional hydrodynamic focusing with a single sheath flow in a single-layer microfluidic device. Lab Chip 9(21):3155–3160. https://doi.org/10.1039/b910712f

Li B, Qiu Y, Glidle A, McIlvenna D, Luo Q, Cooper J, Shi HC, Yin HB (2014) Gradient microfluidics enables rapid bacterial growth inhibition testing. Anal Chem 86(6):3131–3137. https://doi.org/10.1021/ac5001306

Lu MQ, Ho YP, Grigsby CL, Nawaz AA, Leong KW, Huang TJ (2014) Three-dimensional hydrodynamic focusing method for polyplex synthesis. ACS Nano 8(1):332–339. https://doi.org/10.1021/nn404193e

Lyu Y, Yuan X, Glidle A, Fu Y, Furusho H, Yang T, Yin H (2020) Automated Raman based cell sorting with 3D microfluidics. Lab Chip 20(22):4235–4245. https://doi.org/10.1039/D0LC00679C

Mao XL, Waldeisen JR, Huang TJ (2007) "Microfluidic drifting'''—implementing three-dimensional hydrodynamic focusing with a single-layer planar microfluidic device." Lab Chip 7(10):1260–1262. https://doi.org/10.1039/b711155j

Mao X, Nawaz A A, Lin S-C S, Lapsley M I, Zhao Y, McCoy J P, El-Deiry W S and Huang T J (2012) An integrated, multiparametric flow cytometry chip using "microfluidic drifting" based

three-dimensional hydrodynamic focusing. Biomicrofluidics 6 (2):024113–024113–9. https://doi.org/10.1063/1.3701566

Mao XL, Nawaz AA, Lin SCS, Lapsley MI, Zhao YH, McCoy JP, El-Deiry WS, Huang TJ (2012) An integrated, multiparametric flow cytometry chip using "microfluidic drifting" based three-dimensional hydrodynamic focusing. Biomicrofluidics 6 (2) https://doi.org/10.1063/1.3701566

McIlvenna D, Huang WE, Davison P, Glidle A, Cooper J, Yin HB (2016) Continuous cell sorting in a flow based on single cell resonance Raman spectra. Lab Chip 16(8):1420–1429. https://doi.org/10.1039/c6lc00251j

Meineke G, Hermans M, Klos J, Lenenbach A, Noll R (2016) A microfluidic opto-caloric switch for sorting of particles by using 3D-hydrodynamic focusing based on SLE fabrication capabilities. Lab Chip 16(5):820–828. https://doi.org/10.1039/c5lc01478f

Nawaz AA, Zhang XJ, Mao XL, Rufo J, Lin SCS, Guo F, Zhao YH, Lapsley M, Li P, McCoy JP, Levine SJ, Huang TJ (2014) Sub-micrometer-precision, three-dimensional (3D) hydrodynamic focusing via "microfluidic drifting." Lab Chip 14(2):415–423. https://doi.org/10.1039/c3lc50810b

Nolan GP, Fiering S, Nicolas JF, Herzenberg LA (1988) Fluorescence-activated cell analysis and sorting of viable mammalian-cells based on beta-D-galactosidase activity after transduction of Escherichia-coli lacz. Proc Natl Acad Sci USA 85(8):2603–2607. https://doi.org/10.1073/pnas.85.8.2603

Shen YG, Yalikun Y, Tanaka Y (2019) Recent advances in microfluidic cell sorting systems. Sens Actuators B-Chem 282:268–281. https://doi.org/10.1016/j.snb.2018.11.025

Simonnet C and Groisman A (2005) Two-dimensional hydrodynamic focusing in a simple microfluidic device. Applied Physics Letters 87 (11):https://doi.org/10.1063/1.2046729

Skommer J, Akagi J, Takeda K, Fujimura Y, Khoshmanesh K, Wlodkowic D (2013) Multiparameter Lab-on-a-Chip flow cytometry of the cell cycle. Biosens Bioelectron 42:586–591. https://doi.org/10.1016/j.bios.2012.11.008

Song Y, Yin H and Huang W E (2016) Raman activated cell sorting. Current Opinion in Chemical Biology 33 8. https://doi.org/10.1016/j.cbpa.2016.04.002

Wang D, He P, Wang Z, Li G, Majed N, Gu AZ (2020) Advances in single cell Raman spectroscopy technologies for biological and environmental applications. Curr Opin Biotechnol 64:218–229. https://doi.org/10.1016/j.copbio.2020.06.011

Wolff A, Perch-Nielsen IR, Larsen UD, Friis P, Goranovic G, Poulsen CR, Kutter JP, Telleman P (2003) Integrating advanced functionality in a microfabricated high-throughput fluorescent-activated cell sorter. Lab Chip 3(1):22–27. https://doi.org/10.1039/b209333b

Xu CX, Wang M, Yin XF (2011) Three-dimensional (3D) hydrodynamic focusing for continuous sampling and analysis of adherent cells. Analyst 136(19):3877–3883. https://doi.org/10.1039/c1an15019g

Yasukawa T, Glidle A, Nomura M, Cooper JM (2005) Fabrication of robust 2-D and 3-D microfluidic networks for lab-on-a-chip bioassays. J Microelectromech Syst 14(4):839–846

Yin HB, Marshall D (2012) Microfluidics for single cell analysis. Curr Opin Biotechnol 23(1):110–119. https://doi.org/10.1016/j.copbio.2011.11.002

Yuan XF, Couto JM, Glidle A, Song YQ, Sloan W, Yin HB (2017) Single-cell microfluidics to study the effects of genome deletion on bacterial growth behavior. Acs Synthetic Biol 6(12):2219–2227. https://doi.org/10.1021/acssynbio.7b00177

Zhou J, Tu C, Liang Y, Huang B, Fang Y, Liang X, Papautsky I, Ye X (2018) Isolation of cells from whole blood using shear-induced diffusion. Sci Rep 8(1):9411. https://doi.org/10.1038/s41598-018-27779-2

Zhou Y, Ma Z, Ai Y (2018) Sheathless inertial cell focusing and sorting with serial reverse wavy channel structures. Microsyst Nanoeng 4(1):5. https://doi.org/10.1038/s41378-018-0005-6

Zhou J, Mukherjee P, Gao H, Luan Q, Papautsky I (2019) Label-free microfluidic sorting of microparticles. APL Bioeng 3(4):041504. https://doi.org/10.1063/1.5120501